The Journal of Chemical Physics

RESEARCH ARTICLE | JULY 11 2023

Few-body hydrodynamic interactions probed by optical trap pulling experiment

Julian Lee ; Kyle Cotter ; Ibrahim Elsadek ; Matthew J. Comstock ; Steve Pressé

J. Chem. Phys. 159, 024201 (2023)
https://doi.org/10.1063/5.0148096

The Journal of Chemical Physics ARTICLE pubs.aip.org/aip/jcp

Few-body hydrodynamic interactions probed by optical trap pulling experiment

Cite as: J. Chem. Phys. 159, 024201 (2023); doi: 10.1063/5.0148096
Submitted: 28 February 2023 • Accepted: 15 June 2023 •
Published Online: 11 July 2023

Julian Lee,[1] Kyle Cotter,[2] Ibrahim Elsadek,[2] Matthew J. Comstock,[2,a)] and Steve Pressé[3,a)]

AFFILIATIONS

[1]Department of Bioinformatics and Life Science, Soongsil University, Seoul 06978, South Korea
[2]Department of Physics and Astronomy, Michigan State University, East Lansing, Michigan 48824, USA
[3]Department of Physics, Arizona State University, Tempe, Arizona 85287, USA

[a)]**Authors to whom correspondence should be addressed:** mjcomsto@msu.edu and spresse@asu.edu

ABSTRACT

We study the hydrodynamic coupling of neighboring micro-beads placed in a multiple optical trap setup allowing us to precisely control the degree of coupling and directly measure time-dependent trajectories of entrained beads. We performed measurements on configurations with increasing complexity starting with a pair of entrained beads moving in one dimension, then in two dimensions, and finally a triplet of beads moving in two dimensions. The average experimental trajectories of a probe bead compare well with the theoretical computation, illustrating the role of viscous coupling and setting timescales for probe bead relaxation. The findings also provide direct experimental corroborations of hydrodynamic coupling at large, micrometer spatial scales and long, millisecond timescales, of relevance to, e.g., microfluidic device design and hydrodynamic-assisted colloidal assembly, improving the capability of optical tweezers, and understanding the coupling between micrometer-scale objects within a living cell.

I. INTRODUCTION

Forces between solid bodies immersed in fluid are mediated through hydrodynamic interactions,[1] and the effects of such interactions abound across physical[2–4] and biological systems.[5] Although theories of hydrodynamic interaction have been constructed,[6–18] most of their experimental corroborations have relied on indirect methods such as the analysis of collective motions of diffusing colloidal particles[19–29] or by examining the coupled thermal fluctuations of two-body systems.[30–35]

Previously, stationary optical traps have provided a means by which to probe hydrodynamic interactions.[31,33] For typical optical trap stiffnesses and solvent viscosity, bead relaxation times occur on ~1 ms timescales, i.e., timescales over which thermally induced bead motion correlations decay.[31] However, sound propagation[33] was shown to be an important contributor to hydrodynamic coupling,[33] these observations remain indirect as they rely on correlated thermal motion over ~10 nm rather than the prolonged motion of beads over milliseconds. This leaves us to wonder whether theory and simulation accurately model longer lengthscales.

In this work, rather than using beads in stationary optical traps, we probe hydrodynamic coupling by directly measuring the trajectories of micrometer-sized beads in one stationary optical trap (probe bead) in the presence of one or two scan beads in the vicinity pulled using moving optical traps. Using this setup, we directly measure prolonged probe bead displacements of micrometer size on 0.1–1 s timescales. In doing so, we capture the onset of viscous coupling, its development, the resulting probe bead entrainment, and subsequent relaxation manifest at larger spatial and longer temporal scales away from equilibrium.

The scales we monitor are relevant to the self-assembly of colloidal spheres, naturally mediated through hydrodynamic interactions[2,36] and, as we will see, interpolate between results at much faster timescales for single trapped optical beads, e.g., Ref. 37, and bulk bead experiments, e.g., Refs. 2 and 11, on mechanisms underlying assembly.

Of equal, and practical, importance is understanding the hydrodynamic coupling of beads held at short distances, as we explore here, which is relevant in extending tweezer experiments to higher resolution.[38] So far, despite their resolution advantage, short

distances are typically avoided to mitigate the convolution of signals with bead hydrodynamics.[38]

II. THEORY

The dynamics of viscous liquid are described by the linear Navier–Stokes equation,[39]

$$\rho \frac{\partial \mathbf{v}}{\partial t} = -\nabla p + \eta \nabla^2 \mathbf{v}. \tag{1}$$

Alongside the incompressibility condition

$$\rho = \text{ constant} \leftrightarrow \nabla \cdot \mathbf{v} = 0, \tag{2}$$

where ρ, $\mathbf{v}(t,\mathbf{x})$, and $p(t,\mathbf{x})$ are the density, velocity, and pressure fields, $\eta \equiv \rho\nu$ is the dynamic viscosity, and ν is the fluid's kinematic viscosity. When solid bodies are immersed in viscous fluid, the resulting perturbed fluid velocity field is obtained by solving Eqs. (1) and (2), under appropriate boundary conditions on the surface of the solid bodies. By computing the force exerted by such perturbed fields on each solid body, one can obtain the hydrodynamic equation and the resulting dynamical equation of motion for the solid bodies.[1] As a special case, the equation of motion for hard spheres moving in viscous fluid has previously been derived[1,6–9,14,40–42] (see the supplementary material for details). It is clear that, after integrating out fluid degrees of freedom, the resulting dynamic equation for the positions and orientations of the solid bodies is generally non-Markovian, and the future evolution is not solely determined by the current positions and velocities of the bodies but their history as well.[41–43] This naturally manifests as a frequency dependent friction coefficient for the beads, and the equation for the Fourier modes of N beads coupled through hydrodynamic interactions takes the form[33,41,42]

$$i\omega \mathbf{M}\mathbf{U}(\omega) = -\boldsymbol{\zeta}(\omega)\mathbf{U}(\omega) + \mathbf{F}, \tag{3}$$

where the vector $\mathbf{U}(\omega)$ is a $3N$ dimensional vector representing the Fourier mode of the particle velocity, $\mathbf{M}$ is a $3N \times 3N$ diagonal matrix with $M_{3i-2,3i-2} = M_{3i-1,3i-1} = M_{3i,3i} = m_i$ $(i = 1, \ldots, N)$ being the mass of the i-th body, and $\boldsymbol{\zeta}(\omega)$ is a $3N \times 3N$ friction coefficient matrix with $\mathbf{F}$ a vector of dimension $3N$ representing external forces, including trap force and random thermal force.

For beads with identical mass $m_i = m$ and radius a, the velocities of the beads relax to their stationary values determined by the external forces around $\tau_B = \frac{m}{\zeta_0} = \frac{2\rho_b a^2}{9\rho_f \nu}$, where $\zeta_0 = 6\pi\eta$ is the single body friction coefficient at zero frequency, with ρ_b and ρ_f being the densities of the bead and the fluid, respectively. In most of the optical trap experiments including the current work, where microbeads are used, the viscosity of the fluid is similar to that of water, and the density of the bead is of similar order to that of the solvent, $a \sim 0.5$ μm, $\frac{\rho_b}{\rho_f} \sim 1$, $\nu \sim 10^{-6}$ m^2/s, leading to $\tau_B \sim 1$ μs. The same order of magnitude argument applies for beads of slightly different sizes and masses. Thus, to describe motions at ms timescales, we may safely neglect M, leading to[31,33]

$$\mathbf{U}(\omega) = [\boldsymbol{\zeta}(\omega)]^{-1}\mathbf{F}. \tag{4}$$

The timescales over which hydrodynamic memory is relevant, in turn, are dictated by $\tau_{\text{hyd}} = \frac{R^2}{\nu}$, where R is the typical distance between objects.[33] This timescale roughly coincides with the time required for a transverse fluid wave to cover the distance between both beads. In the current work, the distance between beads evolves with time peaking at around $R \sim 6$ μm, leading to $\tau_{\text{hyd}} \lesssim 4$ μs. Therefore, memory is also irrelevant, and the ensuing friction coefficient matrix inverse can be approximated in the form $[\boldsymbol{\zeta}(\omega)]^{-1} \sim \boldsymbol{\mu}\delta(\omega)$, where $\boldsymbol{\mu}$ is termed the mobility tensor.[1] Equation (4) then takes the form[44]

$$\frac{d\mathbf{X}}{dt} = \boldsymbol{\mu}\mathbf{F}, \tag{5}$$

where the $3N$-dimensional vector X represents particle positions. The mobility tensor $\boldsymbol{\mu}$ is normally expressed as a power series in $\epsilon \equiv r/R$, where r is each sphere's radius, and R is the distance between them.[1,6,7,40] Defining $\tilde{\boldsymbol{\mu}}_{ij} \equiv 6\pi\eta\boldsymbol{\mu}_{ij}$, where $i,j = A, B,$ and C index spheres with corresponding radii a, b, and c, we have

$$\begin{aligned}
\tilde{\boldsymbol{\mu}}_{AA} &= a^{-1}\boldsymbol{I} - \frac{15b^3}{4R_{AB}^4}\hat{\mathbf{e}}_{AB}^T\hat{\mathbf{e}}_{AB} - \frac{15c^3}{4R_{AC}^4}\hat{\mathbf{e}}_{AC}^T\hat{\mathbf{e}}_{AC} + O(\epsilon^6), \\
\tilde{\boldsymbol{\mu}}_{AB} &= \frac{3}{4R_{AB}}(\boldsymbol{I} + \hat{\mathbf{e}}_{AB}^T\hat{\mathbf{e}}_{AB}) + \frac{a^2+b^2}{4R_{AB}^3}(\boldsymbol{I} - 3\hat{\mathbf{e}}_{AB}^T\hat{\mathbf{e}}_{AB}) \\
&\quad - \frac{15c^3}{8R_{AC}^2R_{CB}^2}\left(1 - 3(\hat{\mathbf{e}}_{AC}^T \cdot \hat{\mathbf{e}}_{CB})^2\right)\hat{\mathbf{e}}_{AB}\hat{\mathbf{e}}_{CB} + O(\epsilon^6),
\end{aligned} \tag{6}$$

where $\hat{\mathbf{e}}_{ij}$ is the unit column vector connecting the i and j spheres, and $\boldsymbol{I}$ is the unit tensor. The expression for $\tilde{\boldsymbol{\mu}}_{AC}$ is obtained from that for $\tilde{\boldsymbol{\mu}}_{AB}$ by exchanging B and C labels. We explicitly verified that the addition of terms truncated here does not result in visible changes in computed bead trajectories. It is also now straightforward to obtain the mobility for beads A and B, by taking the limit of $R_{AC}, R_{BC} \to \infty$ in Eq. (6)

$$\begin{aligned}
\tilde{\boldsymbol{\mu}}_{AA} &= a^{-1}\boldsymbol{I} - \frac{15b^3}{4R_{AB}^4}\hat{\mathbf{e}}_{AB}^T\hat{\mathbf{e}}_{AB} + O(\epsilon^6), \\
\tilde{\boldsymbol{\mu}}_{AB} &= \frac{3}{4R_{AB}}(\boldsymbol{I} + \hat{\mathbf{e}}_{AB}^T\hat{\mathbf{e}}_{AB}) + \frac{a^2+b^2}{4R_{AB}^3}(\boldsymbol{I} - 3\hat{\mathbf{e}}_{AB}^T\hat{\mathbf{e}}_{AB}) + O(\epsilon^6).
\end{aligned} \tag{7}$$

III. EXPERIMENTAL SETUP

Hydrodynamic coupling between individual microspheres (2.16 μm diameter polystyrene beads) was investigated by measuring the motion of a "probe bead" held in a fixed position trap adjacent to a "scan bead" that quickly moved away and then back toward the probe bead [e.g., as shown in Fig. 1(a)]. A home-built high-resolution optical tweezers instrument was used, constructed, and operated generally as described in Ref. 45 and more specifically as in Ref. 46 and as shown in Fig. S4 in the supplementary material. Three optical traps were formed deep in solution (i.e., away from cover glass) with two scanning traps flanking a fixed position probe bead trap. Traps were precisely manipulated via timesharing a single

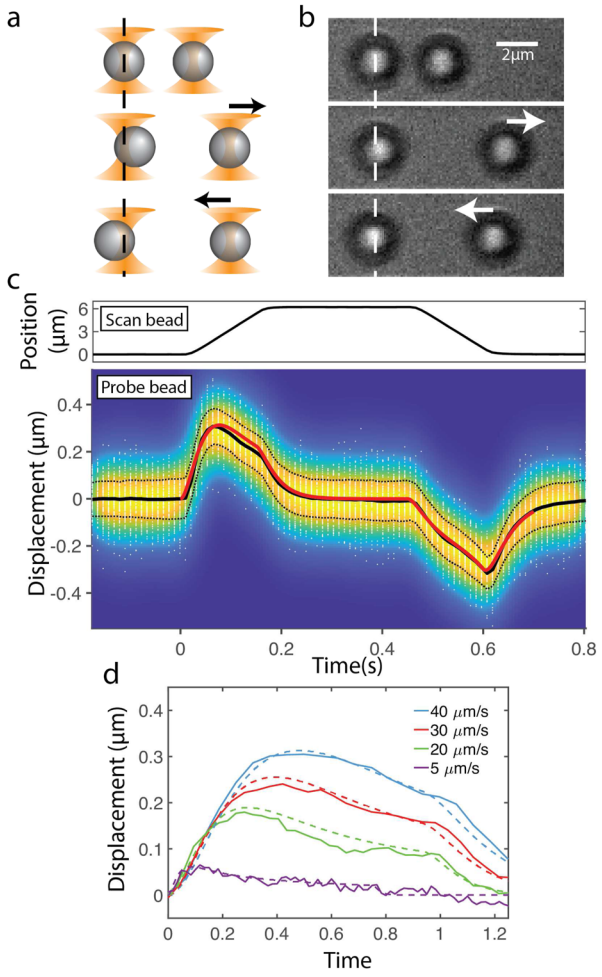

FIG. 1. Two bead linear scan data. (a) Cartoon illustrating the general two bead setup. Optical traps (orange cones) hold microbeads (gray spheres), not to scale. A trap moves a scan bead in the *x*-direction away (middle frame) and then backs toward (bottom frame) a probe bead held in a fixed trap. (b) Images of the linear scanning experiment as in (a). The dashed line indicates the fixed trap position and the probe bead zero displacement as a guide to the eye. The white arrows indicate the scan direction. (c) Linear scan data. Average displacement in the *x*-direction of the scan bead (Upper) and the probe bead (Lower: Black line). The white dots in the lower panel are the actual displacements of the probe beads for each scan, and the background color maps the displacement distribution for one example bead set. The black dashed lines represent the rms of all individual bead sets combined in quadrature. The red line is the simulated bead trajectory. (d) Probe bead displacement (solid line) and corresponding simulated trajectories (dashed lines) for varying scan speeds. The time is normalized so that $t = 0$ is the start of the scan and $t = 1$ is the end of the scan. The same set of beads is used for all curves, and each curve results from the average of 100 individual scans. See Fig. S10 for graphs in unscaled time.

976 nm laser using a two-axis acousto optic deflector (IntraAction DTD-274HD6C) controlled via a direct digital RF synthesis and the field programmable gate array (FPGA) method. Each trap in sequence was on for a duration of 5 μs, and there were no programmed pauses between trap on cycles, i.e., trap 1 is on for 5 μs, then immediately trap 1 turns off and trap 2 turns on for 5 μs, and then immediately trap 2 turns off and trap 3 turns on for 5 μs, etc. Thus, the duty cycle for each trap is 1/3. The AOD switching time is <1 μs. For all experiments, two scanning traps begin flanking the probe bead fixed trap with all three traps arranged in a line, and a scan is initiated by moving the two scanning traps in mirror trajectories away from and then back toward the probe bead trap. For the linear scans, the two scanning traps remain in a line with the probe bead trap [as in Fig. 1(a)], while for the shear scans, the two traps move orthogonally to the initial alignment [as in Fig. 2(a)]. For two-bead experiments, only a single scan trap is occupied by a bead (i.e., the other scan trap is empty), while for three-bead experiments, both scan traps are occupied by beads. We kept the empty third trap on in the two-bead experiments for consistency across all experiments and also to minimize the possible net force applied by the scan traps on the probe bead (i.e., the possible forces applied from the flanking traps directly on the probe bead are always in opposite directions and would cancel). Bead positions were measured via imaging using a CMOS camera (Thorlabs CS165MU) at 92 fps (10.9 ms per frame), which was synchronized with the scans via a signal from the FPGA. The probe bead trap stiffness (nominally 0.85 pN/μm) was minimized to maximize the measured deflection of the probe bead in response to scan bead hydrodynamic coupling. The trap stiffness for each individual bead was calibrated via the standard equipartition method [i.e., using the root-mean-square (rms)] of the bead's Brownian motion and also confirmed by measuring the bead's viscous relaxation time constant within the trap (see Fig. S5 and the associated text in the supplementary material for further details on the trap calibration). The relaxation trajectory of a single bead (i.e., without adjacent scan beads) was well-fit by a single exponential decay over the full range of bead motion, which confirmed that the traps behaved as linear Hookean springs over the relevant bead displacement range. Note that this trap stiffness is the effective trap stiffness, which due to timesharing, is the instantaneous trap stiffness multiplied by the trap duty cycle. Since the time during which each trap is turned off is 10 μs, which is much shorter than the observational time scale of ~ms where the average trajectory of the beads is studied, the optical trap can be modeled as a potential with an effective spring constant. Control measurements were performed with alternate bead and scan configurations to confirm that the measured displacements of the probe bead are due to entrainment with the scan beads rather than spurious trap interactions (See Figs. S6 and S7 in the supplementary material).

IV. RESULTS

We directly detected and recorded the trajectories of the probe bead in response to the fluid flow generated by the scan bead. The simplest perturbation to the probe bead is produced by an experimental configuration where a single bead is scanned in 1D along the line connecting probe and scan beads (subsequently referred to as "two-bead linear scans"). Figure 1(b) shows a sequence of images from an example of an experiment with a probe bead in a fixed position trap on the left and a scan bead in a scanning trap on the right. The beads are assumed to be identical (as we later average over multiple experimental repetitions involving different probe and scan beads). The upper image of Fig. 1(b) shows the initial positions of the trapped beads before initiating the scan, with a closest distance

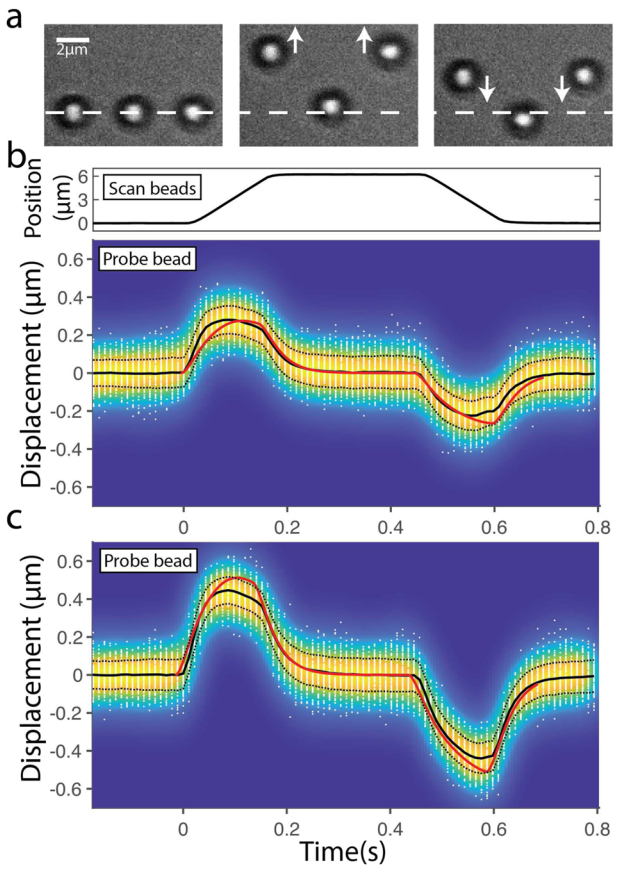

FIG. 2. Two- and three-bead shear scan data. (a) Example images of a three-bead shear mode scanning experiment. For a two-bead shear scanning experiment, the right-side scanning bead would be absent. The dashed line indicates both the probe bead's fixed trap position as well as the initial scan bead trap positions. The white arrows indicate the scan directions (up and down in the *y*-direction). (b) and (c) illustrate shear scan data with displacement in the *y*-direction shown. (b) Upper: Average position of a 2.16 μm scan bead. (b) Lower and (c) Displacement of a 2.16 μm probe bead for two- and three-bead shear scan experiments, respectively. The black line is the displacement trajectory averaged over 11 and 19 unique bead sets for (b) and (c), respectively, with 100 repeated scans each. The white dots are the actual bead displacements for each scan, and the background color maps the displacement distribution for one example bead set. The black dashed lines represent the rms of all individual bead sets combined in quadrature. The red line is the simulated bead trajectory.

between the probe and scan surfaces of 1 μm. The middle image shows a frame of the scan where the scan bead is moving quickly (40 μm/s) away from the probe bead, and the probe bead can be seen clearly displaced from the fixed trap minimum toward the scanning bead (≈300 nm displacement). The lower image shows a frame during the reversal of the scan, where the scan bead is now moving quickly (same speed) toward the probe bead, and the probe bead can be seen clearly displaced from the fixed trap pushed away from the approaching scan bead (≈300 nm displacement).

The complete time trajectory of the entrainment of the probe bead in response to scan bead motion is shown in Fig. 1(c). The solid black line shows the average probe bead displacement in the horizontal direction (i.e., along the scan direction) vs time. Since there is about 10% uncertainty in the bead diameter, we removed the bias introduced by the fact that the actual bead diameter is not exactly 2.16 μm by repeating the experiment on 19 different bead pairs. For each bead pair, the scan was repeated 100 times with a 200 ms delay between successive scans. We then obtained the average trajectory over these 1900 experiments. At $t = 0$, the scan bead starts moving away at a constant speed of 40 μm/s until halting 6 μm away at $t = 0.15$ s. In response, the probe bead is entrained by the scan bead (positive displacement) as the fluid flow induced by the moving scan bead flows past the probe bead and exerts a force on it in turn. The probe bead is much slower than the scanning bead, its average speed being ~6 μm/s from $t = 0$ until it reaches the maximum displacement of ~0.3 μm around $t \sim 0.05$ s. As such, hydrodynamic interactions decrease with time due to the growing inter-bead distance, whereas the opposing force of the trap increases. The trap force takes over the hydrodynamic interaction after $t \sim 0.05$ s, leading to a gradual relaxation of the probe bead back toward the center of the fixed trap for the remaining 2/3 of the scan duration. The probe bead displacement trajectory and maxima depend only weakly on the exact initial probe-scan bead separation (See Fig. S8 in the supplementary material). Upon halting the scan at $t = 0.15$ s, the probe bead rapidly relaxes to the center of the trap following an exponential decay. After a 0.3 s pause (sufficient to ensure the probe bead is completely relaxed), the scan reverses and the scan bead moves back toward the probe bead at a constant speed of 40 μm/s. The probe bead is now pushed away from the scan bead (negative displacement). Note that this probe bead motion is not the mirror of the prior positive displacement motion. Indeed, since the push at the second scan starts at a larger inter-bead distance compared to the pull at the first scan, the hydrodynamic coupling is also weaker initially and becomes large only at the later stage where the restoring force of the trap becomes large. Consequently, the distance from the trap center increases slowly and monotonically until it reaches ~0.3 μm in the negative direction at 0.6 s, at which point the reverse scan stops, leading to an exponential decay in displacement afterward. After a 0.4 s pause, the scan repeats for a total of 100 cycles. The Brownian fluctuations of the bead position are significant compared to the maximum mean displacement trajectories [the rms of probe bead fluctuations is 80 nm while the maximum displacement is 300 nm, as seen directly by comparing individual trajectories and the distribution of these from Fig. 1(c)]. The theory, as described above, simulates the probe-bead-scan-bead hydrodynamic coupling reproducing the predicted mean probe bead trajectory (in red), which easily fits within the noise of the Brownian fluctuations.

Note that we do not include the effects of photophoretic and thermophoretic forces in our analysis.[47–50] In contrast to beads coated with gold nanoparticles, purely dielectric beads such as ones used here are considered effectively as cold particles where photophoretic and thermophoretic effects are negligible.[50] More importantly, due to the axial symmetry of each trap, any such forces in the directions transverse to the trap axis will cancel away when we average over the fluctuations.

Since the magnitude of the hydrodynamic interaction is directly proportional to the speed of the objects moving in the fluid [See Eq. (7) in the supplementary material], we expect the inter-bead coupling to be weakened if we decrease the speed of the scan bead.

The average trajectory of a single bead set for the linear scan is shown in Fig. 1(d), along with computational results (See also Fig. S9 in the supplementary material for graphs in unscaled time). We indeed see that the maximal displacement of the probe bead decreases with the speed of the scan bead, in accordance with the theoretical prediction. Since we are averaging over only 100 trajectories for a single bead set, the effect of the thermal noise is more prominent than the data shown in (c).

In order to test the effect of the hydrodynamic interaction on 2D motion, whose modeling is expected to be more challenging, we also performed "shear" configuration experiments where beads flanking the probe bead are scanned orthogonally to the initial line connecting the probe and scan beads. Figure 2(a) shows a sequence of images demonstrating the shear mode scan configuration for the case of two flanking scan beads. Nearly all scan parameters are identical to the linear scan mode parameters (Fig. 1): all beads are nominally identical, the initial trap positions are identical, with a closest distance between the probe and scan bead surfaces of 1 μm, and the scanning trap speed is 40 μm/s. The only difference is the direction of the scan (which is vertical rather than horizontal). The experiments were repeated with either one or two flanking beads.

The complete trajectories of the displacement of the probe bead in response to the shear mode scanning beads with either one or two scanning beads are shown in Figs. 2(b) and 2(c), respectively. The solid black lines show the average probe bead vertical displacement (i.e., parallel to the direction of the scan) vs time, averaged over many bead pair replicates, where each replicate is an average of 100 repeated scans of the same beads. At $t = 0$, the scanning bead starts moving away at a constant speed of 40 μm/s until halting 6 μm away at $t = 0.15$ s. As for the linear scans, the probe bead follows the scan beads. For two flanking scan beads scanning in the same direction (as shown), the probe bead motion is completely vertical, whereas for a single scan bead, there is a slight horizontal displacement following the scan bead (Fig. S10 in the supplementary material). If two scanning beads scan in opposite directions (i.e., one upward and one downward), no displacement of the probe bead is observed as expected (Figs. S6 and S7 in the supplementary material). Both the initial speed ($\approx$9.5 μm/s) and the maximum displacement (0.45 μm) of the probe bead are about 50% greater with two scan beads compared to those with one scan bead ($\approx$6 μm/s and 0.28 μm). The probe bead is pulled toward the retreating scan bead during the initial scan (positive displacement). After the intermediate scan pause, the probe bead is pushed away from the approaching scan beads (negative displacement). Again, this trajectory following the pause and reversal of direction of the scan bead is not a simple reversal of the trajectory preceding the pause, for the same reasons as in the case of the linear scan. The relaxation of the probe bead at scan halts is exponential with more or less the same time constants in all cases (Data not shown).

Both 2D fluid coupling effects on shear scans and three-body interactions in the case of the two scanning beads necessarily involve a greater degree of approximation than the linear two bead scans. Concretely, three-body motility tensors necessarily compound the approximations already present in the two-body tensor, while, in shear scans, incomplete modeling of external torques acting on the beads by the optical trap may contribute to the bead's 2D motion. Despite these modeling challenges, we found that probe bead trajectories predicted by the theory still lie within the uncertainty of the probe bead Brownian fluctuations, though the mean does not match as closely as for the linear case.

V. CONCLUSIONS

In this work, we studied two- and three-body hydrodynamic interactions by directly probing the trajectory of a microbead in a stationary optical trap hydrodynamically entrained by neighboring microbeads. In contrast to previous work where ~10 nm-scale thermal fluctuations of beads were analyzed to obtain information on hydrodynamic interaction,[31,33] here we averaged out thermal fluctuations to obtain trajectories or prolonged motion on μm lengthscales. Therefore, the current results provide independent and direct corroboration of hydrodynamic interactions. Furthermore, we probed three-body interactions in addition to two-body interactions. The resulting data agree with theoretical predictions within Brownian noise. Since, prior to averaging, our raw data contains thermal noise, it would also be interesting to compare the properties of such noise to theoretical predictions. The theory for moving beads within viscous fluid supplemented by thermal fluctuations is the object of future investigation, as currently no method exists for computing thermal fluctuations around spheres whose distance varies in time.

What is more, we have limited ourselves to the effects of entrainment manifest from rectilinear motion, though rotational diffusion and transfer of rotational chirality are also of immediate interest to questions of colloidal self-assembly.[2] Just as with thermal fluctuations, our results can be said to be rotationally and thermally averaged. Indeed, for rotational diffusion, torques acting on the beads cannot be known precisely. This is because the angular orientation and rotation of a trapped bead lie outside the scope of the existing measurement capabilities of high-resolution optical tweezers.

Recently, there has been interest in active colloids, where particles in the fluid self-propel with fuel.[51–55] In addition to hydrodynamic interactions, such particles also interact via various phoretic interactions induced by anisotropy in chemical concentrations, temperatures, and electric fields in their vicinity. Various approaches exist to model such systems, and theoretical frameworks similar to ours have been used[52,55] even making phoretic interactions explicit. Direct experimental corroboration with few-body systems, such as done here, can help inspire the study of additional effects. In particular, the agreement between theory and experiment suggests that hydrodynamic interaction far-field expansions[6,7] remain helpful even as objects fall within distances of each other comparable to their size and that frameworks such as the one proposed here can be expanded to include other effects.

Finally, the conclusions drawn here are relevant to optical tweezer experiments, where beads are often limited to operating at a far distance from one another. Such experiments are performed precisely to eliminate bead–bead coupling effects. Yet for short bead–bead distances, as the spring constant of the tether typically goes inversely with the end-to-end tether distance,[38] models to account for coupling under this scenario are a key step toward improving the tether's sensitivity to the dynamics of the single molecule.

SUPPLEMENTARY MATERIAL

The supplementary material contains additional details on derivation and experiments. It is organized by first elaborating on details of the theory, highlighting, for instance, the result of ignoring higher order terms in our model. We then turn to the experimental setup, providing, for instance, a layout of the dual-trap optical tweezer experiment.

ACKNOWLEDGMENTS

J.L. was supported by the National Research Foundation of Korea, funded by the Ministry of Science and ICT (Grant No. NRF-2020R1A2C1005956). K.C., I.E., and M.J.C. were supported by the NSF (Grant No. MCB-1919439). S.P. was supported by the NIH (Grant Nos. R01GM130745, R01GM134426, and R35GM148237).

AUTHOR DECLARATIONS

Conflict of Interest

The authors have no conflicts to disclose.

Author Contributions

Julian Lee: Formal analysis (equal); Funding acquisition (equal); Investigation (equal); Methodology (equal); Software (equal); Visualization (equal); Writing – original draft (equal); Writing – review & editing (equal). **Kyle Cotter**: Conceptualization (equal); Data curation (supporting); Funding acquisition (equal); Investigation (equal); Project administration (equal); Validation (supporting); Writing – original draft (equal); Writing – review & editing (equal). **Ibrahim Elsadek**: Conceptualization (equal); Data curation (supporting); Funding acquisition (equal); Investigation (equal); Methodology (equal); Project administration (equal); Supervision (equal); Validation (supporting); Visualization (equal); Writing – original draft (equal); Writing – review & editing (equal). **Matthew J. Comstock**: Conceptualization (equal); Data curation (equal); Funding acquisition (equal); Investigation (equal); Methodology (equal); Project administration (equal); Supervision (equal); Validation (equal); Visualization (equal); Writing – original draft (equal); Writing – review & editing (equal). **Steve Pressé**: Conceptualization (equal); Data curation (equal); Funding acquisition (equal); Investigation (equal); Project administration (equal); Validation (equal); Writing – original draft (equal); Writing – review & editing (equal).

DATA AVAILABILITY

The data that support the findings of this study are available from the corresponding author upon reasonable request.

REFERENCES

[1] S. Kim and S. J. Karrila, *Microhydrodynamics: Principles and Selected Applications* (Dover Publications, Inc., New York, 2005).
[2] Z. Shen, A. Würger, and J. S. Lintuvuori, "Hydrodynamic self-assembly of active colloids: Chiral spinners and dynamic crystals," Soft Matter **15**, 1508–1521 (2019).
[3] F. Snijkers, R. Pasquino, and J. Vermant, "Hydrodynamic interactions between two equally sized spheres in viscoelastic fluids in shear flow," Langmuir **29**, 5701–5713 (2013).
[4] V. Lisy, J. Tothova, and A. V. Zatovsky, "Long-time dynamics of Rouse–Zimm polymers in dilute solutions with hydrodynamic memory," J. Chem. Phys. **121**, 10699 (2004).
[5] T. Ando and J. Skolnick, "Crowding and hydrodynamic interactions likely dominate in vivo macromolecular motion," Proc. Natl. Acad. Sci. U. S. A. **107**, 18457–18462 (2010).
[6] P. Mazur, "On the motion and Brownian motion of n spheres in a viscous fluid," Physica A **110**, 128–146 (1982).
[7] P. Mazur and W. van Saarloos, "Many-sphere hydrodynamic interactions and mobilities in a suspension," Physica A **115**, 21–57 (1982).
[8] S. Kim, "Stokes flow past three spheres: An analytic solution," Phys. Fluids **30**, 2309–2314 (1987).
[9] B. Cichocki, B. U. Felderhof, K. Hinsen, E. Wajnryb, and J. Blawzdziewicz, "Friction and mobility of many spheres in Stokes flow," J. Chem. Phys. **100**, 3780–3790 (1994).
[10] J. T. Padding and A. A. Louis, "Hydrodynamic and Brownian fluctuations in sedimenting suspensions," Phys. Rev. Lett. **93**, 220601 (2004).
[11] J. T. Padding and A. A. Louis, "Hydrodynamic interactions and Brownian forces in colloidal suspensions: Coarse-graining over time and length scales," Phys. Rev. E **74**, 031402 (2006).
[12] T. Geyer and U. Winter, "An $O(N^2)$ approximation for hydrodynamic interactions in Brownian dynamics simulations," J. Chem. Phys. **130**, 114905 (2009).
[13] R. R. Schmidt, J. G. H. Cifre, and J. G. de la Torre, "Comparison of Brownian dynamics algorithms with hydrodynamic interaction," J. Chem. Phys. **135**, 084116 (2011).
[14] H. J. Wilson, "Stokes flow past three spheres," J. Comput. Phys. **245**, 302–316 (2013).
[15] A. Donev and E. Vanden-Eijnden, "Dynamic density functional theory with hydrodynamic interactions and fluctuations," J. Chem. Phys. **140**, 234115 (2014).
[16] A. Daddi-Moussa-Ider and S. Gekle, "Hydrodynamic interaction between particles near elastic interfaces," J. Chem. Phys. **145**, 014905 (2016).
[17] G. Jung and F. Schmid, "Frequency-dependent hydrodynamics interaction between two solid spheres," Phys. Fluids **29**, 126101 (2017).
[18] J. Lee, S. L. Seyler, and S. Pressé, "Hydrodynamic interaction facilitates the unsteady transport of two neighboring vesicles," J. Chem. Phys. **151**, 094108 (2019).
[19] J. X. Zhu, D. J. Durian, J. Müller, D. A. Weitz, and D. J. Pine, "Scaling of transient hydrodynamic interactions in concentrated suspensions," Phys. Rev. Lett. **68**, 2559–2562 (1992).
[20] M. H. Kao, A. G. Yodh, and D. J. Pine, "Observation of Brownian motion on the time scale of hydrodynamic interactions," Phys. Rev. Lett. **70**, 242–245 (1993).
[21] A. J. C. Ladd, H. Gang, J. X. Zhu, and D. A. Weitz, "Time-dependent collective diffusion of colloidal particles," Phys. Rev. Lett. **74**, 318 (1995).
[22] D. T. Valley, S. A. Rice, B. Cui, H. M. Ho, H. Diamant, and B. Lin, "Pair diffusion in quasi-one- and quasi-two-dimensional binary colloid suspensions," J. Chem. Phys. **126**, 134908 (2007).
[23] S. Novikov, S. A. Rice, B. Cui, H. Diamant, and B. Lin, "Hydrodynamic interactions in ribbon channels: From quasi-one-dimensional to quasi-two-dimensional behavior," Phys. Rev. E **82**, 031403 (2010).
[24] J. R. Villanueva-Valencia, J. Santana-Solano, E. Sarmiento-Gómez, S. Herrera-Velarde, J. L. Arauz-Lara, and R. Castañeda-Priego, "Long-time dynamics and hydrodynamic correlations in quasi-two-dimensional anisotropic colloidal mixtures," Phys. Rev. E **98**, 062605 (2008).
[25] B. Lin, B. Cui, J.-H. Lee, and J. Yu, "Hydrodynamic coupling in diffusion of quasi–one-dimensional Brownian particles," Europhys. Lett. **57**, 724–730 (2002).
[26] B. Cui, H. Diamant, and B. Lin, "Screened hydrodynamic interaction in a narrow channel," Phys. Rev. Lett. **89**, 188302 (2002).
[27] B. Cui, H. Diamant, B. Lin, and S. A. Rice, "Anomalous hydrodynamic interaction in a quasi-two-dimensional suspension," Phys. Rev. Lett. **92**, 258301 (2004).

[28]K. Misiunas, S. Pagliara, E. Lauga, J. R. Lister, and U. F. Keyser, "Nondecaying hydrodynamic interactions along narrow channels," Phys. Rev. Lett. **115**, 038301 (2015).
[29]Z. Zheng, X. Xu, Y. Wang, and Y. Han, "Hydrodynamics couplings of colloidal ellipsoids diffusing in channels," J. Fluids Mech. **933**, A40 (2022).
[30]J. C. Crocker, "Measurement of the hydrodynamic corrections to the Brownian motion of two colloidal spheres," J. Chem. Phys. **106**, 2837 (1997).
[31]J. C. Meiners and S. R. Quake, "Direct measurement of hydrodynamic cross correlations between two particles in an external potential," Phys. Rev. Lett. **82**, 2211 (1998).
[32]E. R. Dufresne, T. M. Squires, M. P. Brenner, and D. G. Grier, "Hydrodynamic coupling of two Brownian spheres to a planar surface," Phys. Rev. Lett. **85**, 3317–3320 (2000).
[33]S. Henderson, S. Mitchell, and P. Bartlett, "Propagation of hydrodynamic interactions in colloidal suspensions," Phys. Rev. Lett. **88**, 088302 (2002).
[34]S. Martin, M. Reichert, H. Stark, and T. Gisler, "Direct observation of hydrodynamic rotation-translation coupling between two colloidal spheres," Phys. Rev. Lett. **97**, 248301 (2006).
[35]R. Di Leonardo, E. Cammarota, G. Bolognesi, H. Schäfer, and M. Steinhart, "Three-dimensional to two-dimensional crossover in the hydrodynamic interactions between micron-scale rods," Phys. Rev. Lett. **107**, 044501 (2011).
[36]J. Ha, Y. S. Kim, K. Jiang, R. Siu, and S. Tawfick, "Hydrodynamic elastocapillary morphing of hair bundles," Phys. Rev. Lett. **125**, 254503 (2020).
[37]R. Huang, I. Chavez, K. M. Taute, B. Lukić, S. Jeney, M. G. Raizen, and E. L. Florin, "Direct observation of the full transition from ballistic to diffusive Brownian motion in a liquid," Nat. Phys. **7**, 576–580 (2011).
[38]C. J. Bustamante, Y. R. Chemla, S. Liu, and M. D. Wang, "Optical tweezers in single-molecule biophysics," Nat. Rev. Methods Primers **1**, 25 (2021).
[39]L. D. Landau and E. M. Lifshitz, *Fluid Mechanics* (Pergamon Press, Oxford, 1987).
[40]G. J. Kynch, J. Fluid Mech. **5**, 193 (1959).
[41]A. M. Ardekani and R. H. Rangel, "Unsteady motion of two solid spheres in Stokes flow," Phys. Fluids **18**, 103306 (2006).
[42]B. U. Felderhof, "Retarded hydrodynamic interaction between two spheres immersed in a viscous incompressible fluid," Phys. Fluids **31**, 053604 (2019).
[43]S. L. Seyler and S. Pressé, "Long-time persistence of hydrodynamic memory boosts microparticle transport," Phys. Rev. Res. **1**, 032003(R) (2019).
[44]We explicitly checked that the addition of the memory effect does not lead to any visible change in the computational results for two-bead cases (data not shown).
[45]K. C. Neuman and S. M. Block, "Optical trapping," Rev. Sci. Instrum. **75**, 2787–2809 (2004).
[46]R. Yadav, K. B. Senanayake, and M. J. Comstock, "High-resolution optical tweezers combined with multicolor single-molecule microscopy," in *Optical Tweezers: Methods and Protocols*, edited by A. Gennerich (Springer US, New York, 2022), pp. 141–240.
[47]A. S. Desyatnikov, V. G. Shvedov, A. V. Rode, W. Krolikowski, and Y. S. Kivshar, "Photophoretic manipulation of absorbing aerosol particles with vortex beams: Theory versus experiment," Opt. Express **17**, 8201–8211 (2009).
[48]V. G. Shvedov, A. V. Rode, Y. V. Izdebskaya, A. S. Desyatnikov, W. Krolikowski, and Y. S. Kivshar, "Giant optical manipulation," Phys. Rev. Lett. **105**, 118103 (2010).
[49]M. Xuan, Z. Wu, J. Shao, L. Dai, T. Si, and Q. He, "Near infrared light-powered Janus mesoporous silica nanoparticle motors," J. Am. Chem. Soc. **138**, 6492–6497 (2016).
[50]J. Frueh, S. Rutkowski, T. Si, Y.-X. Ren, M. Gai, S. I. Tverdokhlebov, G. Qiu, J. Schmitt, Q. He, and J. Wang, "Direct measurement of thermophoretic and photophoretic force acting on hot micromotors with optical tweezers," Appl. Surf. Sci. **549**, 149319 (2021).
[51]H. R. Vutukuri, B. Bet, R. van Roij, M. Dijkstra, and W. T. S. Huck, "Rational design and dynamics of self-propelled colloidal bead chains: From rotators to flagella," Sci. Rep. **7**, 16758 (2017).
[52]N. Yoshinaga and T. B. Liverpool, "Hydrodynamic interactions in dense active suspensions: From polar order to dynamical clusters," Phys. Rev. E **96**, 020603(R) (2017).
[53]J. Stürmer, M. Seyrich, and H. Stark, "Chemotaxis in a binary mixture of active and passive particles," J. Chem. Phys. **150**, 214901 (2019).
[54]I. P. Madden, L. Wang, J. Simmchen, and E. Luijten, "Hydrodynamically controlled self-organization in mixtures of active and passive colloids," Small **18**, 2107023 (2022).
[55]A. Zöttl and H. Stark, "Modeling active colloids: From active Brownian particles to hydrodynamic and chemical fields," Annu. Rev. Condens. Matter Phys. **14**, 109–127 (2023).